International Journal of Astronomy 2023, 12(1): 1-11
DOI: 10.5923/j.astronomy.20231201.01

Nutation and Chandler Wobble in a Model of the Rotating and Undulating Curved Surface of Space-time in the Solar System

Adrián G. Cornejo

Electronics and Communications Engineering from Universidad Iberoamericana, Santa Rosa 719, CP 76138, Querétaro, Mexico

Abstract Based on the Schwarzschild metric, the Flamm's paraboloid of revolution, and the Lense–Thirring precession, we explore a model in which the entire Solar System rotates and undulates the curved surface of space-time that forms it. This model considers the representation of a curved space-time surface as an undulated four-dimensional surface in rotation with vertex at the Sun. With this model, the rate of apsidal precession, axial precession, nutation and Chandler wobble of the Earth can be predicted from a rotating and undulating Solar System scenario. In this approximation, nutation and Chandler wobble can be described as arbitrary oscillations in the Earth's orbit as it traverses an undulating space-time surface while orbits. According to this model, planets and other celestial bodies in the Solar System would oscillate when orbiting around the Sun, forming the rate of the observed nutation and Chandler wobble of the Earth and Mars while the system is in rotation. The undulations on the curved space-time surface would resemble consecutive waves as in a fluid in rotation. The curved space-time geometry of the Solar System can be observed from pictures taken from orbiting spacecraft. Then, we estimate in this model the orientation of the Earth's North Pole with respect to curved space-time, considering that the North Pole must point towards the inner Solar System.

Keywords Schwarzschild metric, Flamm's paraboloid, Lense–Thirring precession, Nutation, Chandler wobble

1. Introduction

The entire Solar System is considered to remain static while the planets orbit around the Sun. However, what effects would there be if the entire Solar System rotates and undulates the curved surface of space-time that forms it? And would such effects match some of the known observations? In General Relativity [1], the Einstein field equations describe the metric of the four-dimensional space-time static surface expressed by the stress-energy tensor. The concise form of the Einstein field equation is defined as

$$G_{\mu\nu} = R_{\mu\nu} - \frac{1}{2}Rg_{\mu\nu} = \frac{8\pi G}{c^4}T_{\mu\nu}\ , \qquad (1)$$

where $G_{\mu\nu}$ is the Einstein tensor, $R_{\mu\nu}$ is the Ricci tensor, G is the Newtonian constant of gravity, c is the speed of light in vacuum, $T_{\mu\nu}$ is the stress-energy tensor at a point P, and the indices μ, ν run 1, 2, 3, 4. The stress-energy tensor is a range 2 tensor that can be described as a matrix of type 4 × 4, and represents the content of matter and energy (including particles, radiation, fields, and energies) at a point P on the four-dimensional static surface. An observer in a homogeneous and isotropic universe, moving so that the universe is observed to be isotropic, would measure the stress-energy tensor as

$$T_{\mu\nu} = \begin{pmatrix} \rho & 0 & 0 & 0 \\ 0 & p & 0 & 0 \\ 0 & 0 & p & 0 \\ 0 & 0 & 0 & p \end{pmatrix}, \qquad (2)$$

where the components on the diagonal define the energy density ρ and pressure p. This diagonal form is a consequence of symmetry. According to General Relativity, space-time can be considered a four-dimensional static surface (spherical for simplicity) with some elasticity to be deformed in the presence of a massive body. The geometry that is formed with this equation is that of a spherical surface that can be curved towards a central point P, in which matter and energy are concentrated (see Figure 1). According to Eq. (1), curvature is directly proportional to the quantity of matter and energy at the point P, among others local variables as pressure. Thus, space-time static surface would remain "flat" (i.e. no deformed) when there is not enough matter and energy on the surface concentrated at a point P [see Figure 2(a)]. On the other hand, space-time surface could be curved in different ways in the presence of enough matter and energy at a point P.

* Corresponding author:
adriang.cornejo@gmail.com (Adrián G. Cornejo)
Received: Feb. 19, 2023; Accepted: Mar. 4, 2023; Published: Mar. 21, 2023
Published online at http://journal.sapub.org/astronomy

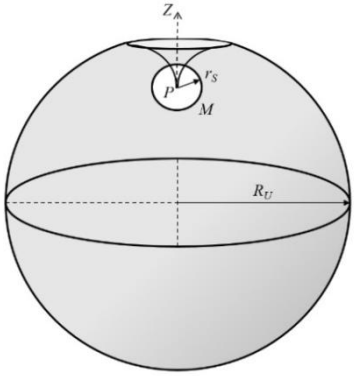

Figure 1. Three-dimensional representation of the geometry of the Einstein's equation that describes the universe as a spherical surface (for simplicity) supporting enough matter-energy at the point *P* to curve the spherical surface. R_U is the radius of the universe

The surface can take the form of a static concavity [see Figure 2(b)] by a significative mass such as planets and moons, among other celestial bodies. In the case of a star or a black-hole singularity at a point *P*, there would be a static surface as a paraboloid [see Figure 2(c)].

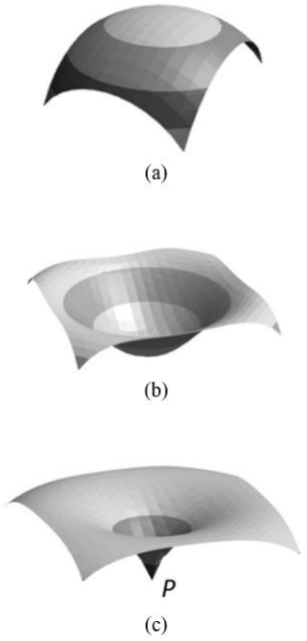

Figure 2. Three-dimensional representation of three possible forms of curvature of space-time static surface, according to General Relativity: (a) The so-called "flat" universe in the Einstein equations for vacuum, when $R_{\mu\nu} = 0$. (b) Enough matter and energy to curve space-time static surface, as in the case of moons and planets, among other celestial bodies. (c) Curvature of the space-time static surface due to a star or a black-hole singularity at a point *P*

1.1. Elliptical Orbits in the Schwarzschild Metric

An exact solution of the Einstein field equations was developed by Schwarzschild [2], which describes a four-dimensional curved space-time static surface in the vacuum for a static (non-rotating) and spherically symmetric star or black-hole singularity. The Schwarzschild metric resembles a Flamm's paraboloid of revolution about the *Z*-axis [3] (similar to a "curved cone") which does not include the Schwarzschild radius. It can be derived as follows. The Euclidean metric in the cylindrical coordinates (r, φ, z) is written as

$$ds^2 = dz^2 + dr^2 + r^2 d\phi^2. \quad (3)$$

Letting the static surface be described by the function $z = z_{(r)}$, the Euclidean metric can be written as

$$ds^2 = \left[1 + \left(\frac{dz}{dr}\right)^2\right] dr^2 + r^2 d\phi^2. \quad (4)$$

Comparing this with the Schwarzschild metric in the equatorial plane ($\theta = \pi/2$) at a fixed time (where t = constant, $dt = 0$) and $r_s = 2GM/c^2$ is Schwarzschild radius, we get

$$ds^2 = \left(1 - \frac{r_S}{r}\right)^{-1} dr^2 + r^2 d\phi^2 \,, \quad (5)$$

yields an integral expression for $z_{(r)}$ given as

$$z_{(r)} = \int \frac{dr}{\sqrt{\frac{r}{r_S} - 1}} = 2r_S \sqrt{\frac{r}{r_S} - 1} + \mathrm{c} \,, \quad (6)$$

whose solution for $r > r_S$ is the Flamm's paraboloid given as

$$z_{(r)}^2 = 4r_S^2 \left(\frac{r}{r_S} - 1\right) = 4r_S(r - r_S). \quad (7)$$

Term $(r - r_s)$ form the limit that excludes the Schwarzschild radius of the static surface, so it is a limit of the formed geometry. As an approximation about limits, we can rewrite this limit as

$$z_{(r)}^2 = 4r_S[r]|_{r_S}^{r} = 4r_S \Delta r = 4r_S r_\Delta \,, \quad (8)$$

with the conditions that $r > r_S$ and r_Δ can be reintegrated as $(r - r_s)$ if required. According to this geometry, considering $r_\Delta{}^2 = x^2 + y^2$, we can write this equation as the static surface of a paraboloid (with vertex at the origin) in the form

$$\frac{x^2}{a^2} + \frac{y^2}{b^2} = \frac{z^4}{c^4} \frac{1}{(4r_S)^2} \,. \quad (9)$$

The orbital paths followed by a freefalling object moving on the tangent plane to the curvature can be calculated through the intersection of the paraboloid and the tangent plane. The corresponding tangent plane is given by the first differential of the Flamm's paraboloid, written as

$$z = 2\sqrt{r_S(r - r_S)} = 2\sqrt{r_S r_\Delta} \,, \quad (10)$$

where *z* is the vertical axis and $4r_S$ remains constant (for each massive body). The tangent to the curvature for any point on the curve up to a radial length r_0 from the origin, in cylindrical coordinates, is given by

$$dz = \frac{2\sqrt{r_S}}{2\sqrt{r_0}} (r_\Delta + r_0). \quad (11)$$

And considering only the projection on the *XZ*-plane, we obtain

$$dz = \frac{\sqrt{x_S}}{\sqrt{x_0}} (x + x_0). \quad (12)$$

Reducing common terms and considering that $r^2 = x^2 + y^2$, yields

$$\sqrt{r} = \sqrt[4]{x^2 + y^2} = \frac{\sqrt{x_S}}{\sqrt{x_0}}(x + x_0). \quad (13)$$

Getting the fourth power and rearranging, hence

$$\frac{x^2 x_0^2}{x_S^2 (x + x_0)^4} + \frac{y^2 x_0^2}{x_S^2 (x + x_0)^4} = 1, \quad (14)$$

which is the equation of an ellipse on a tangent plane to the curvature (see Figure 3). This explains Kepler's first law in General Relativity. As known, a body moving linearly with constant velocity maintains constant angular momentum around any point, and sweeps out equal areas in equal time intervals, that is, dA/dt = constant. Then, when its trajectory is tilted, for example, by the surface deformation due to a central mass, a body sweeps equal areas in equal time intervals while orbiting the central mass, so the body would change its velocity during the orbit. Which is in accordance with Kepler's second law.

1.2. Tilt of the Orbital Plane and the Ecliptic in the Schwarzschild Metric

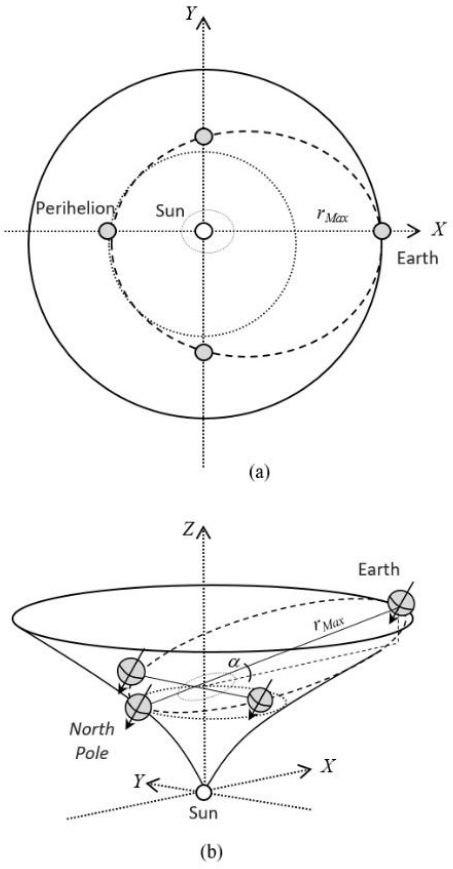

Figure 3. (a) Top view representation of the Earth's orbit on the *XY*-plane, in a planar geometry of the Solar System. (b) Three-dimensional representation of the lateral view of the considered curved geometry of space-time static surface of the Solar System with vertex at the Sun, and with the Earth's orbit on the tangent plane to the curvature, according to the Schwarzschild metric

In the Flamm's paraboloid, the tilt of an orbital plane with respect to the *XZ*-plane is the tangent to the curve at the furthest point of the orbit with respect to the focus. In the Solar System, the distance $r_{Max} = a(1 + e)$ is the maximum Planet-Sun distance during aphelion, where a is the semi-major axis of the ellipse and e its eccentricity.

A right triangle can be formed in the *XZ*-plane with the maximum distance (r_{Max}) as hypotenuse (see Figure 4), given as

$$r_{Max}^2 = x_0^2 + z_F^2 , \quad (15)$$

$$z_F = z_0 - z_{f1} , \quad (16)$$

and in a parabola with vertex at the origin, satisfies

$$z_0 = \sqrt{x_0} . \quad (17)$$

The angle α in radians of the orbital plane on the *XZ*-plane can be obtained as

$$\cos(\alpha) = \frac{x_0}{r_{Max}} , \quad (18)$$

$$\alpha = \arccos\left(\frac{x_0}{r_{Max}}\right) . \quad (19)$$

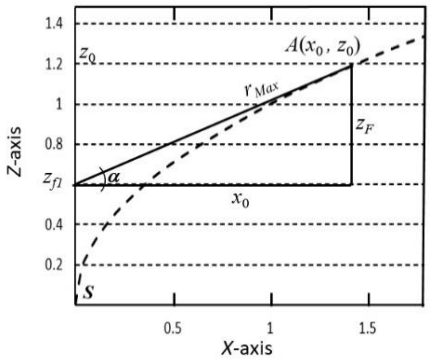

Figure 4. In a curved space-time static surface representation, a right triangle is formed with the maximum distance to the Sun (r_{Max}) as the hypotenuse. The tilt angle α is the tilt of the orbital plane tangent to the curvature in the *XZ*-plane

In the case of the Earth, the maximum Earth-Sun distance is about $r_{Max} = 1.514 \times 10^8$ km. The ecliptic plane is the mean plane of the Earth's orbit around the Sun. This orbital plane is inclined about 23.45° with respect to the plane of the equator [4]. It is the axial tilt or obliquity. The ecliptic plane is considered to be 0° with respect to the tilt of the Earth's orbital plane. Then, the "zero" reference with respect to the *XZ*-plane moves to 23.45°. Thus, we must subtract α_{Earth} to all the determined angles α_n to refer to the ecliptic of the Earth's orbital plane. We can write this condition as

$$\alpha_{Eclip} = |\alpha_n - \alpha_{Earth}|, \quad (20)$$

where α_{Eclip} is the tilt angle of the orbital plane with respect to the ecliptic and α_{Earth} is the tilt angle of the Earth's orbital plane with respect to the *XZ*-plane. Tilt of some celestial bodies with respect to the ecliptic is shown in Table 1, which are the respective orbital inclinations with the ecliptic measured in observations for each celestial body [5]. Figure 5 plots the representation of the respective inclination of some celestial bodies as tangent to the curved static surface in the *XZ*-plane.

Table 1. Tilt with respect to the ecliptic of some celestial bodies, according to the Flamm's paraboloid applied to the known orbital information (with the Sun at the origin)

Description	Mercury	Venus	Earth	Mars	Ceres	Pluto
a (10^8 km)	0.58	1.08	1.49	2.27	4.15	44.35
e (eccentricity)	0.21	0.01	0.02	0.09	0.08	0.18
Maximum distance to the Sun r_{Max} (10^8 km)	0.70	1.09	1.52	2.49	4.46	73.75
x_0 (10^8 km)	0.60	0.97	1.39	2.32	4.35	73.30
z_0 (10^8 km)	0.78	0.99	1.18	1.52	2.09	8.56
z_F (10^8 km)	0.35	0.49	0.60	0.92	0.99	8.10
α_n tilt respect to the XZ-plane (radians)	0.532	0.469	0.409	0.377	0.224	0.110
α_n tilt respect to the XZ-plane (degrees)	30.45	26.84	23.45	21.60	12.86	6.30
α_{Eclip} tilt respect to the ecliptic (degrees)	7.004	3.394	0	1.85	10.59	17.148

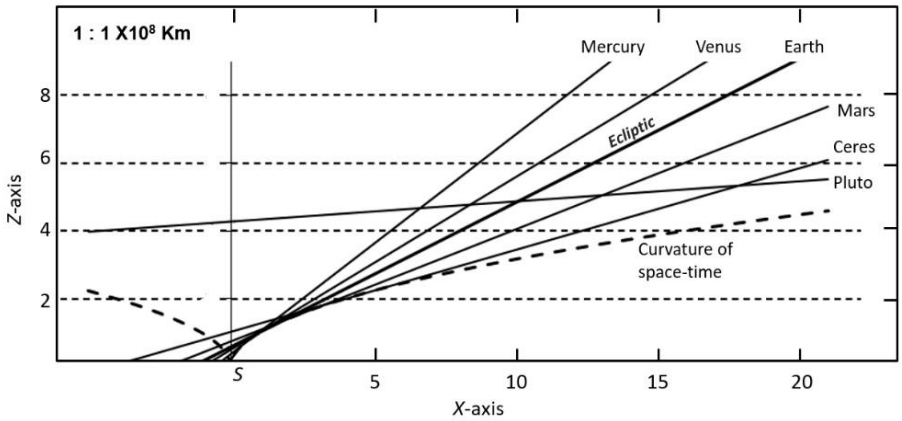

Figure 5. Representation of the tilt of the orbital planes of some celestial bodies as tangents to the four-dimensional curvature of the static surface in the Flamm's paraboloid (dashed line). The Sun (S) at the origin

1.3. Apsidal Precession of the Elliptical Orbits in the Schwarzschild Metric

One of the first predictions of the GTR was the correct calculation to determine the advance of Mercury's perihelion [6]. Since then, this calculation has been developed by different methods, giving the same result. According to the Schwarzschild's metric, the effective potential can be written as

$$V_{(r)} = \frac{\mu c^2}{2}\left[-\frac{r_S}{r} + \frac{a^2}{r^2} - \frac{r_S a^2}{r^3}\right], \tag{21}$$

where r_S is the Schwarzschild radius, μ is the reduced mass and $a = h/c = L/\mu c$ is the length, where h is the specific angular momentum and L is the angular momentum. When $M >> m$, the reduced mass is approximately equal to m. Then, the effective or total force is given as

$$F_{T(r)} = -\frac{V_{(r)}}{dr} = -\frac{mc^2}{r^4}\left[r_S\frac{r^2}{2} - a^2 r + \frac{3}{2}r_S a^2\right], \tag{22}$$

where the last term is the correction from General Relativity. From the Schwarzschild metric, the relativistic approximation to the elliptical orbit of a celestial body around the Sun is given as

$$u'' + u = \left(\frac{3}{2}r_S\right)u^2, \tag{23}$$

$$\frac{d^2u}{d\theta^2} + u = \left(\frac{3GM}{c^2}\right)u^2, \tag{24}$$

where $u = 1/r$. Multiplying by $d\theta$ and reordering, gives

$$\frac{d^2u}{u^2 d\theta^2}d\theta + \frac{u}{u^2}d\theta = \frac{3GMd\theta}{c^2}. \tag{25}$$

Replacing $u = 1/r$ and reducing common terms, yields

$$\left[\frac{d^2(1/r)}{(1/r)^2 d\theta^2} + \frac{(1/r)}{(1/r)^2}\right]d\theta \approx rd\varphi = \frac{3GMd\theta}{c^2}, \tag{26}$$

where $d\varphi$ is the angle of precession, $d\theta = \omega dt$ is the differential of the colatitude radial angle covered by the rotation of the body in the rotating reference frame. Extending Eq. (26) to the Kepler's geometry for a body in elliptical orbit around the Sun at a focus, where in the ellipse $\rho = a(1 - e^2)$, a is the semi-major axis and e is the eccentricity. When the body moves in one revolution ($\theta = 2\pi$ radians), becomes

$$d\varphi = \frac{3GM(2\pi)}{a(1-e^2)c^2} = \frac{6\pi GM}{a(1-e^2)c^2}. \tag{27}$$

Thus, considering the Newtonian equivalence of GM in terms of the period T for an elliptical orbit, defined as

$$GM = \frac{(2\pi)^2 a^3}{T^2}, \tag{28}$$

and replacing in Eq. (27), becomes

$$d\varphi = \frac{3(2\pi)^3 a^2}{c^2 T^2 (1-e^2)} = \frac{24\pi^3 a^2}{c^2 T^2 (1-e^2)}, \tag{29}$$

which is the relativistic equation to calculate the advance of Mercury's perihelion.

It is known that all planets precess, regardless of their distance from the Sun, and this equivalence can be applied to determine the apsidal precession of all other planets in the Solar System, giving the same results as the observations for each planet, respectively.

1.4. Apsidal Precession from the Lense-Thirring Dragging Effect Revisited

Some works [7,8] consider, in a Friedmann–Lemaître (FL) geometry, that both the curvature of space-time surface described by General Relativity and the accelerated expansion of the universe [9,10] considered from the Hubble observations, provide both the dynamics and the curved geometry of space-time surface in the presence of a massive body. However, outside the expansion dynamics of the universe, these possible forms of curved space-time surface are considered static (i.e. no rotational dynamics is considered) around stationary mass distributions. In addition, some works [11-15] consider the scenario in which the entire Solar System would be rotating around a spin axis at the Sun and with a specific angular velocity.

Regarding rotating systems, the gravitation of a spinning spherical massive body of constant density was studied by Lense and Thirring [16]. We can consider the Lense–Thirring precession, which is a relativistic correction to the precession of a rotating body, such as a gyroscope, near a large rotating mass, such as the Earth or the Sun (which has a mass of approximately 1.99×10^{30} kg, and rotational velocity of approximately 1,997 $\mathrm{km \cdot s^{-1}}$) [17]. This effect is due to the rotation of the central mass. It is a prediction of General Relativity consisting of secular precessions of the longitude of the ascending node and the argument of pericentre of a test particle freely orbiting a central spinning mass endowed with angular momentum *S*. The metric is given as

$$ds^2 = \left(1 - \frac{2GM}{rc^2}\right)c^2dt^2 - \left(1 + \frac{2GM}{rc^2}\right)d\sigma^2 + 4G\epsilon_{ijk}S^k\frac{x^i}{c^3r^3}cdt\,dx^j, \quad (30)$$

where ds^2 is the metric, $d\sigma^2 = dx^2 + dy^2 + dz^2 = dr^2 + r^2d\theta^2 + r^2\sin^2\theta d\varphi^2$ is the flat-space line element in three dimensions, $r^2 = x^2 + y^2 + z^2$ is the square of the "radial" position of the observer, c is the speed of light, G is the Newtonian gravitational constant, ϵ_{ijk} is the antisymmetric Levi-Civita symbol,

$$M = \int T^{00}d^3x, \quad (31)$$

is the mass of the rotating body, and

$$S_k = \int \epsilon_{klm}x^lT^{m0}d^3x, \quad (32)$$

is the angular momentum of the rotating body, where $T^{\mu\nu}$ is the energy-momentum tensor.

The above is the weak-field approximation of the full solution of the Einstein equations for a rotating star or black-hole singularity, known as the Kerr metric [18]. Kerr found a more general solution to Einstein's field equations, obtaining the geometry of curved space-time out of a mass distribution with no charge and rotation about one of its axes. In this solution, the zero-rotation limit corresponds to the Schwarzschild solution. Thus, having the curvature of space-time derived by Schwarzschild and the dynamics of rotation, due to the swirling curvature of space-time itself associated with rotating bodies. The Kerr metric that describes the dynamics of curved space-time outside of a rotating star or black-hole singularity is given as

$$ds^2 = dt^2 - \frac{\rho^2}{\Delta}dr^2 - \rho^2d\theta^2 - (r^2 + a^2)\sin^2\theta d\varphi^2 - \frac{2Mr}{\rho^2}(dt - a\sin^2\theta d\varphi)^2. \quad (33)$$

where

$$a = \frac{J}{M}, \quad \rho^2 = r^2 + a^2\cos(\theta), \quad \Delta = r^2 - 2Mr + a^2. \quad (34)$$

The term a describes the rotation of the spinning star or black-hole singularity, where J is its angular momentum, M its total mass-energy content, and (r, θ, φ) are the usual polar coordinates.

Note that if we carry out the expansion of the fifth (quadratic) term in the Kerr metric, we obtain what is known as an oblic term, the $dtd\varphi$ term. The appearance of this term in the metric is responsible for what is now known as the Lense-Thirring effect, with which the reference frames close to the rotating star or black-hole singularity are dragged along with it.

The frame-dragging effect can be demonstrated solving for geodesics; these will then exhibit a Coriolis force-like term, except that, in this case, the force is not fictional, but is due to frame dragging induced by the rotating body. Thus, an (instantly) radially infalling geodesic at the equator will satisfy the equation

$$\frac{rd^2\alpha}{dt^2} + \frac{2GJ}{c^2r^3}\frac{dr}{dt} = 0, \quad (35)$$

where t is the time, α is the longitudinal angle (azimuthal angle) and $J = \| S \| = Mr^2\omega$ is the magnitude of the angular momentum of the spinning massive body, where ω is the angular velocity of the rotating coordinate system. The above can be compared to the standard equation for motion subject to the Coriolis acceleration (a_C), giving

$$r\alpha'' + 2\omega\frac{dr}{dt} = 0, \quad (36)$$

$$\frac{rd^2\alpha}{dt^2} + 2\omega v = 0, \quad (37)$$

$$a_C + 2\omega^2r = 0, \quad (38)$$

where $v = \omega r$ is the radial velocity.

When the observer is not in radial motion, i.e. if $dr/dt = 0$, there is no effect on the observer. In this scenario, the frame-dragging effect will cause a gyroscope to precess. The rate of precession is given by

$$\Omega^k = \frac{G}{c^2r^3}\left[S^k - \frac{3(S\cdot x)x^k}{r^2}\right] = \frac{GS^k}{c^2r^3} - \frac{3G(S\cdot x)x^k}{c^2r^3(r^2)}, \quad (39)$$

where Ω is the angular velocity of the precession, Ω^k is one of its components, S_k is the angular momentum of the

spinning body, $S \cdot x$ is the ordinary flat-metric inner product of the position and the angular momentum. That is, when the gyroscope's angular momentum relative to the fixed stars is L^i, then it precesses as

$$\frac{dL^i}{dt} = \epsilon_{ijk}\,\Omega^j L^k. \tag{40}$$

The rate of precession is given by

$$\epsilon_{ijk}\,\Omega^k = \Gamma_{ij0}\,, \tag{41}$$

where Γ_{ij0} is the Christoffel symbol for the above metric. Extending the angular momentum as $\| S \| = Mr^2\omega$ in the second term (as positive) of Eq. (39), yields

$$\Omega^k = \frac{3G(Mr^2\omega\cdot x)x^k}{c^2r^3(r^2)}, \tag{42}$$

and writing this equation with respect to the radial position of the observer on the *XY*-plane, for the component when $k = 1$, gives

$$\Omega_{(r)} = \frac{3G(Mr^2\omega\cdot r)r}{c^2r^3(r^2)}. \tag{43}$$

Reducing common terms and having the angular velocity of the precession in function of time, yields

$$\Omega = \frac{d\varphi}{dt} = \frac{3GM\omega}{c^2r}, \tag{44}$$

$$d\varphi = \frac{3GM\omega dt}{c^2r} = \frac{3GMd\theta}{c^2r}, \tag{45}$$

where $d\varphi$ is the rate of angle of precession, $d\theta = \omega dt$ is the differential of the radial angle covered by the rotation of the body in the rotating reference frame. This is the same equation that the derived in Eq. (26), since it is also derived from a rotating system analysis. As also considered in previous works [12,15], extending Eq. (45) to the Newtonian equivalence given in Eq. (28) for a body in elliptical orbit around the Sun at a focus. When the body moves in one revolution ($\theta = 2\pi$ radians), becomes

$$d\varphi = \frac{3(2\pi)^3a^2}{c^2T^2(1-e^2)} = \frac{24\pi^3a^2}{c^2T^2(1-e^2)}, \tag{46}$$

which is the relativistic equation to calculate the precession of Mercury's perihelion but derived from the precession in a rotating body (see Figure 6). Thus, this precession is due to the rotation of the system.

It is known that all planets precess, regardless of their distance from the Sun, and this equivalence can be applied to determine the apsidal precession for all planets in the Solar System, giving the same results as the observations for each respective apsidal precession. Expression in polar coordinates for the ellipse with the pole at a focus, also including the rate of apsidal precession, is given by

$$r_{Max} = \frac{a(1-e^2)}{1-e\cdot\cos(\theta+d\varphi)} = \frac{a(1-e^2)}{1-e\cdot\cos(\omega t+\Omega \mathrm{d}t)}, \tag{47}$$

where r_{Max} is the maximum distance from the body to the centre of rotation (i.e. during the aphelion), $\theta = \omega t$ and $d\varphi = \Omega dt$.

1.5. Axial Precession in the Rotating Reference Frame

Considering a model of the rotating Solar System, such a kind of rotation should be perceived from Earth as a change in linear position with respect to the observed "fixed" stars, noting that these would have an apparent periodic circular motion. Indeed, this effect is the observed in axial precession. From Eq. (44) and considering the angular velocity in terms of Coriolis acceleration, yields

$$\Omega_C = \frac{3GM\omega_C}{c^2r}, \tag{48}$$

where Ω_C and ω_C are in terms of Coriolis acceleration. Thus, writing the magnitude of the Coriolis acceleration from Eq. (37) as

$$|a_C| = 2\omega v, \tag{49}$$

and applying the equivalence between speed and angular velocity ($v = \omega r$), and $v = at$, respectively, the time dependent equation can be written as

$$|a_C| = 2\left(\frac{v}{r}\right)(at). \tag{50}$$

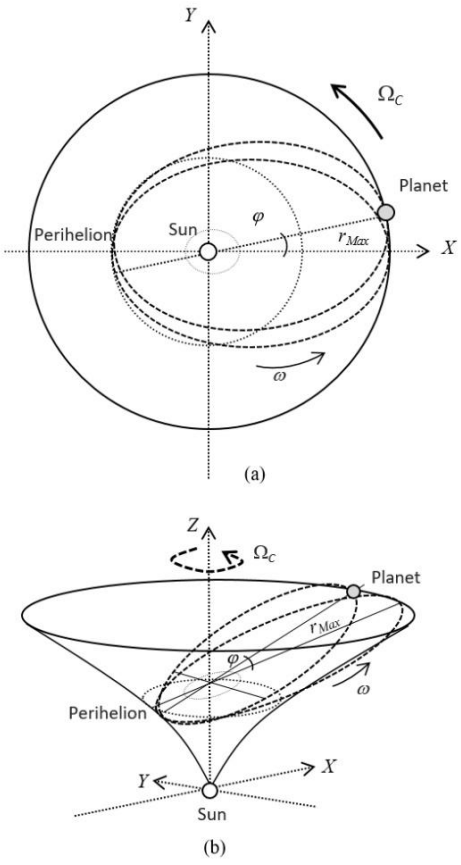

Figure 6. Three-dimensional representation of the apsidal precession (like the precession of Mercury's perihelion) in a four-dimensional rotating reference frame. (a) Top view representation. (b) Lateral view representation

Integrating two times in function of time, neglecting the integration constants in this approximation and simplifying, yields

$$v_C = \int a_C\,dt = 2\left(\frac{va}{r}\right)\int tdt = \left(\frac{va}{r}\right)t^2 + \mathrm{c}\,, \tag{51}$$

$$r_C = \int v_C\,dt = \left(\frac{va}{r}\right)\int t^2dt = \left(\frac{va}{r}\right)\frac{t^3}{3} + \mathrm{c} = v\frac{t}{3}. \tag{52}$$

Simplifying and reordering, yields

$$v_C = \frac{r_C}{t} = \frac{v}{3}, \tag{53}$$

and applying the equivalence $v = \omega r$, gives

$$\omega_C = \frac{v_C}{r} = \frac{v}{3r}. \tag{54}$$

Then, extending from Eq. (38) to the respective terms and replacing Eq. (54) in Eq. (48), we get

$$|a_C| = 2\Omega_C^2 r = \frac{3GM\omega_C}{c^2 r}(\omega_C r) = \frac{3GM}{c^2 r}\left(\frac{v}{3r}\right)^2 r. \tag{55}$$

Simplifying and reordering, yields

$$\Omega_C^2 = \frac{GMv^2}{6c^2 r^3}. \tag{56}$$

As also considered in previous works [13-15], having the apsidal precession from Eq. (46), we must include this precession movement of Earth's orbit in the total angular frequency Ω_T of the system in rotation, giving

$$\Omega_T = \Omega + \Omega_C = \frac{6\pi GM}{a(1-e^2)c^2 t_P} + \left(\frac{GMv^2}{6c^2 r^3}\right)^{\frac{1}{2}}, \tag{57}$$

where t_P is the time in seconds of a sidereal year. For one revolution (2π radians), the total period is written as

$$T_T = \frac{2\pi}{\Omega_T} = \frac{2\pi}{\Omega + \Omega_C}, \tag{58}$$

$$T_T = \frac{2\pi}{\frac{6\pi GM}{a(1-e^2)c^2 t_P} + \left(\frac{GMv^2}{6c^2 r^3}\right)^{\frac{1}{2}}}. \tag{59}$$

For the maximum Earth-Sun distance (r_{Max}) and the related minimum orbital velocity, substituting the Earth-Sun system data [5] in Eq. (59), the total angular frequency equals 7.7255×10^{-12} radians per second (0.0139689° per year), and for one revolution, the total period is 8.133×10^{11} seconds (25,771.5 years), which is according to the observed period of Earth's axial precession, also known as Platonic year.

Since a consequence of the axial precession is a changing pole star, we interpret in this model (as shown in Figure 7) that about the year 2100 AC (point A), Earth's North Pole will be appointing near of the Polaris star (point C). Later, when the Earth travels out by a half period of the Platonic year to the opposite side (point B), Earth's North Pole will appoint near of Vega star (point D) in the year 14000 AC, changing the Earth its position within the Solar System, and resulting in the effect of the axial precession, coinciding with the known observations and predictions. In addition, a body in orbit and rotating around a fixed axis describes a periodic rosette-like path [12]. Then, equation in polar coordinates (Appendix A) can be written as

$$r_{Max} = \frac{a(1-e^2)}{1 - e \cdot cos\,(\omega t + d\Omega t)} \cos(\omega t + \Omega_c t), \tag{60}$$

where r_{Max} is the maximum distance (during aphelion) of the orbiting body from the center of rotation, ω is the angular frequency of the orbit, Ω_C is the total angular frequency of the system, Ω is the angular frequency of apsidal precession, and t is the time. The movement of the body orbiting and rotating forms a rosette-like path (see Figure 7). Thus, the Flamm's paraboloid in rotation can be written in cylindrical coordinates as

$$z^2 = 4r_S(r - r_S)\Omega_C t = 4r_S(r - r_S)\theta. \tag{61}$$

2. Model of Nutation as Undulations Along the Space-Time Surface in the Rotating Reference Frame

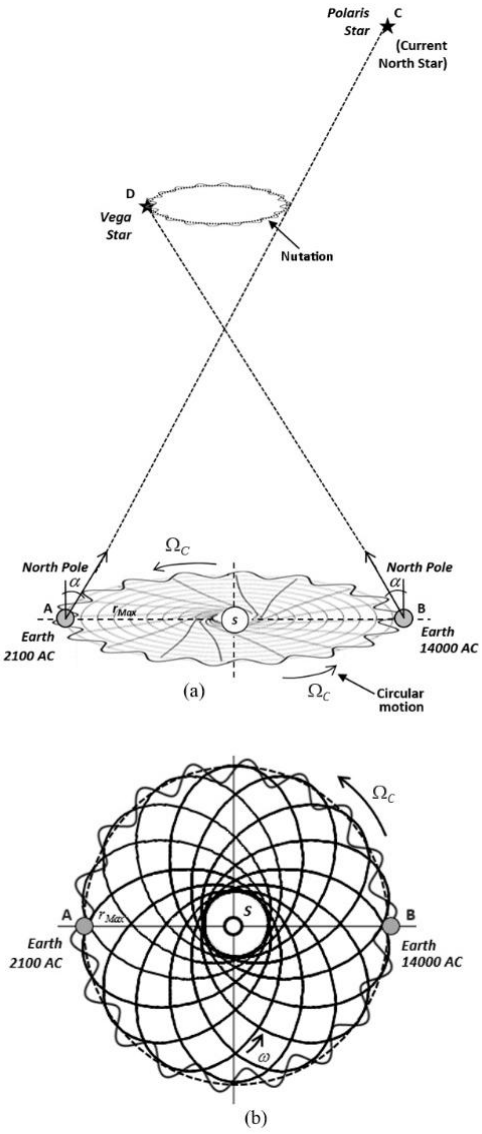

Figure 7. (a) Three-dimensional representation of the path of the Earth orbiting and rotating in a rotating system with undulations to form the observed nutation with respect to the "fixed" stars. (b) Top view representation of the rosette-like path of the Earth orbiting and rotating in a rotating system with undulations to form the observed nutation with respect to the "fixed" stars

Nutation is considered a slight irregular movement in the axis of rotation of symmetrical objects that rotate on their axis [19]. In the case of the Earth, the nutation is superimposed on the axial precession motion and the swaying of the obliquity of the ecliptic so that they are not regular, but rather wavy. The nutation of the Earth causes

that every 18.6 years the axis of rotation of the Earth apparently oscillates up to about 284.28 m (9.2 seconds of arc) on each side of the mean value of the obliquity of the ecliptic.

It is considered that the other planets also produce variations, called perturbations, but these are of a small value to be considered to affect these planetary movements. Since nutation is an additional axial motion superimposed to the axial precession, in this model nutation is considered as the oscillation of the orbit due to the undulations of the space-time surface that a planet follows while orbits. Therefore, we can model the geometry of curved space-time surface in rotation accordingly to the observed nutation. In this model, Earth (as well as the other planets) follow the undulated shape of the rotating curved space-time surface with crests and troughs along the orbital path. To comply with the observed nutation, we arbitrarily add a term which builds the oscillations to the rotating curved space-time surface [20], in order to model and resemble the nutation movement. From Eq. (58), this model can be written as

$$R = r_{Max} + |A\sin(b\theta)|\,, \tag{62}$$

where A = 284.28 m is the amplitude of the undulation and b = 1,385.56 is the number of undulations per cycle (one Platonic year), as shown in Figure 7. This models a curved space-time surface with undulations that satisfies nutation.

3. Model of Chandler Wobble as Undulations Along the Rotating Curved Space-Time Surface

The Chandler wobble or Chandler variation of latitude is a small deviation detected in the Earth's axis of rotation [21]. The Chandler wobble is superimposed on the nutation and on the axial precession motion. It is considered as a nutation. It amounts to change of about 9 m at the point at which the axis intersects the Earth's surface and has a period of 433 days [22].

In the same way, we arbitrarily add a second term which builds the oscillations of the rotating curved space-time surface, in order to model and resemble the Chandler variation. Considering Eqs. (58) and (60), the equation that describes the spinning of the curved space-time surface with crests and troughs along this movement, is modelled as

$$R = r_{Max} + |A_1\sin(b_1\theta)| + |A_2\sin(b_2\theta)|\,, \tag{63}$$

where A_2 = 9 m is the amplitude of the additional undulation and b_2 = 21,724.24 is the number of undulations per cycle (one Platonic year). This model of rotating curved space-time surface with the additional undulations satisfies the Chandler wobble.

3.1. Spiral Behavior in the Dynamics of a Rotating Reference Frame

As also considered in a previous work [15], from Eq. (22) and in the same way as with the equation for classical mechanics scenario to define the orbital velocity, we equate the centrifugal force with the given third term which consider the correction from General Relativity, obtaining

$$m\frac{v^2}{r} = \frac{3GMm\Omega_C^2}{c^2}\,, \tag{64}$$

$$v = \sqrt{\frac{3GMr\Omega_C^2}{c^2}}\,. \tag{65}$$

Furthermore, according to Eq. (41), we can write the angular momentum as $J = Mr^2\Omega_C$, where M is the central mass of the system. Then, the rotational velocity can be calculated by the angular velocity of the system, by its equivalence with angular momentum J, or by the specific angular momentum $j = J/M$ [23], which increases almost linearly with respect to any distance from the nucleus as a function of distance, giving

$$v = \sqrt{\frac{3GM}{c^2r^3}\frac{J^2}{M^2}} = \sqrt{\frac{3GMj^2}{c^2r^3}}\,. \tag{66}$$

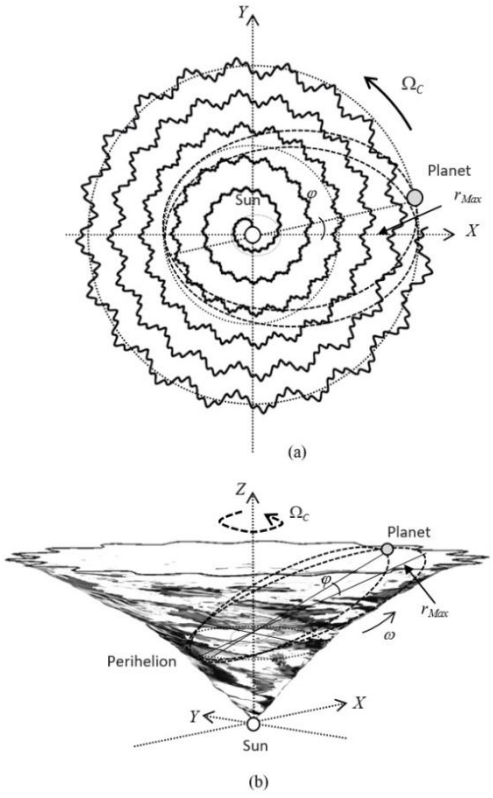

Figure 8. (a) Top view representation of the rotating and undulated curved space-time surface in the Solar System. (b) Three-dimensional representation of the lateral view of the considered rotating and undulated curved geometry of space-time surface in the Solar System, resembling a rotating vortex with crests and troughs and with the vertex at the Sun, and with the Earth's orbit on the tangent plane to the curvature

Having that $\theta = \Omega_C t$ and, for the sake of describing the geometry of this equation, considering the Schwarzschild radius r_s, we write Eq. (64) in polar coordinates as

$$\frac{2v}{3}\left(\frac{r}{t}\right) = \frac{2GMr\Omega_C}{c^2}\left(\frac{v}{r}\right), \tag{67}$$

$$r = \left(\frac{3}{2}\right)\frac{2GM}{c^2}\Omega_C t = \frac{3}{2}r_S\theta\,, \tag{68}$$

which is the equation of a spiral with center at the origin, of the form $r = b\theta$. In this model, Eq. (68) represents the spiral behavior of the rotational dynamics of the space-time surface in the Solar System. Considering Eq. (63), when the system is in rotation, yields

$$R = [r_{Max} + |A_1 \sin(b_1\theta)| + |A_2 \sin(b_2\theta)|]\theta. \quad (69)$$

Then, the rotating surface of this model must have the corresponding geometry to comply with the observed movements of the Earth. From Eq. (61), in cylindrical coordinates, we can write it as

$$z^2 = [4r_S(r - r_S) + |A_1 \sin(b_1\theta)| + |A_2 \sin(b_2\theta)|]\theta\ , \quad (70)$$

which is the equation of Flamm's paraboloid rotating as spiral and with two levels of the undulations of the rotating surface. This equation models a rotating and undulated curved space-time surface in the Solar System, as shown in Figure 8.

3.2. Chandler Wobble of Mars in the Rotating Reference Frame

With radio tracking observations of the Mars Reconnaissance Orbiter, Mars Odyssey and the Mars Global Surveyor spacecraft, the Chandler wobble of Mars was detected. The detected amplitude is 10 cm, the period is 206.9 ± 0.5 days and it is in a nearly circular counterclockwise direction as viewed from the North Pole [24]. Modelling the shape of the rotating space-time surface, adding the Chandler wobble of Mars, it can be consistent with nutation and Chandler wobble in Earth and Mars, as

$$z^2 = [4r_S(r - r_S) + |A_1 \sin(b_1\theta)| + |A_2 \sin(b_2\theta)| + |A_3 \sin(b_3\theta)|]\theta. \quad (71)$$

In general, for n levels of undulations, this model can be written as

$$z^2 = [4r_S(r - r_S) + \sum_{i=0}^{n} |A_i \sin(b_i\theta)|]\theta. \quad (72)$$

In this model, the Chandler wobble of Mars is consistent with a third level of undulations (i = 3), since the Chandler wobble detected on Mars has proportionally more oscillations and smaller amplitude than in the case of Earth (which would indicate that the rate of oscillation could be related to the amount of mass, and to the dynamic scaling of growing interfaces [25]).

4. The Position of the Earth in the Curved Space-time Surface in the Solar System

Considering the image of Earth (moving away from its perihelion) and Jupiter (moving away from its aphelion) during an alignment with Mars, taken on May 8th, 2003 from the Mars Global Surveyor (NASA) orbiting spacecraft pictures [26,27] to graphically determine the direction in which the North Pole of the Earth points with respect to the Solar System.

From this picture and considering that the orbit of Mars is between the orbits of Earth and Jupiter, we note that the Earth's South Pole is fully visible and pointing towards Jupiter, which appears in the image at a great "vertical" distance d from the Earth. This means that the Earth's South Pole must be pointing towards the outer Solar System, while the North Pole must be pointing towards the inner Solar System (see Figure 9). The direction of the Earth's North Pole is also shown in Figure 3(b). Thus, having Jupiter below in the picture and the Earth above (closer to the Sun), the Sun must be positioned at the top of the picture.

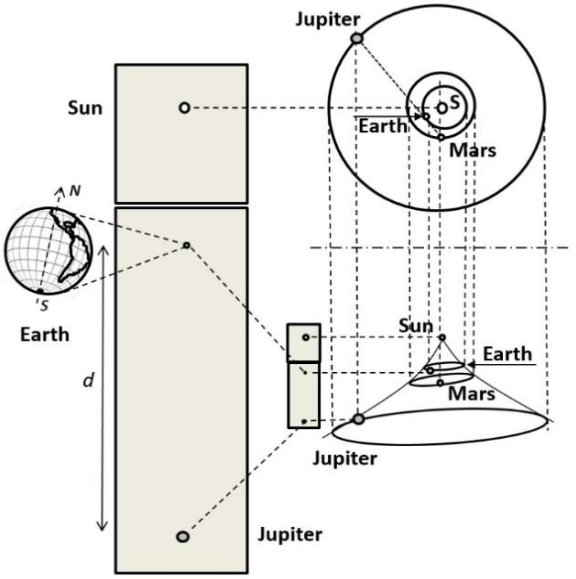

Figure 9. Representation of the isometric projection of the geometry of curved space-time surface in the Solar System from an interpretation of the Mars Global Surveyor picture (May 8, 2003)

In this planetary alignment, if all three planets were in the same plane (for instance, as would be the case of a flat Solar System like a disk), this image could not have been taken from Mars, since in such a case Earth and Jupiter would appear very close (with Jupiter behind Earth). Instead, the image shows Earth and Jupiter very far apart vertically (distance d in Figure 9).

5. Conclusions

The aim of this work is to explore a model of a rotating and undulating curved space-time surface in the Solar System from a post-Newtonian scenario. In this way, the consideration of the rotational and undulation dynamics of the Solar System allows to consider the curved space-time surface to comply with some known movements of the Earth, such as the apsidal precession, axial precession, nutation and Chandler wobble from this scenario. Then, the geometry and rotational dynamics of curved space-time surface in the Solar System is modelled with undulations, in which the orbits can match with the nutation and Chandler wobble, resembling an undulating surface as a rotating vortex in spiral with vertex in the Sun. In this way, the

apsidal precession, the axial precession, nutation and Chandler wobble of the Earth and Mars can be modelled from the Flamm's paraboloid as undulated and in rotational dynamics. From satellite pictures and observations, the position and geometric orientation of the Earth with respect to curved space-time surface can be estimated, considering that the North Pole must point towards the inner Solar System. The next step in proving the dynamics of rotation and undulation of the curved space-time in the Solar System is to make more precise and detailed observations of its angular momentum and relative motion with respect to other celestial bodies, in order to confirm if the way in which space-time rotates and undulates in the Solar System agrees with these considerations and can be predicted by the dynamics described in this model.

ACKNOWLEDGEMENTS

The author would like to thank Professor Sergio S. Cornejo for its review and comments for this work.

Appendix A. The Rosette-Like Path of a Body Orbiting and Rotating Around a Fixed Axis

The elliptical path of a body periodically orbiting around a fixed axis in a static circular reference frame as described by the Kepler's laws shows a simple harmonic oscillator with angular frequency ω. Elliptical path in parametric equations, is given as

$$\begin{aligned} x &= a \cdot \cos(\omega t) \\ y &= b \cdot \sin(\omega t) \end{aligned}, \tag{73}$$

where a is the semi-major axis, b the semi-minor axis and t the parameter.

In addition, elliptical path in a rotating reference frame must be also rotating with angular frequency Ω of the whole system. Thus, a body orbiting and rotating should trace out a simple harmonic motion within the rotating reference frame, which we can be separated into two components with the same frequency, but perpendicular directions out phased by 90° between them. The position of a point in a non-inertial frame in parametric equations is given by

$$\begin{aligned} x' &= x \cdot \cos(\Omega t) - y \cdot \sin(\Omega t) \\ y' &= x \cdot \sin(\Omega t) + y \cdot \cos(\Omega t) \end{aligned}, \tag{74}$$

Thus, replacing x and y terms of Ec. (74) in (73), respectively, the parametric components of a simple harmonic motion for a non-inertial frame are given by

$$\begin{aligned} x' &= a \cdot \cos(\omega t)\cos(\Omega t) - b \cdot \sin(\omega t)\sin(\Omega t) \\ y' &= a \cdot \cos(\omega t)\sin(\Omega t) + b \cdot \sin(\omega t)\cos(\Omega t) \end{aligned}, \tag{75}$$

The given body should follow one of both motions, elliptical or circular orbit; it depends on the relation between the a and b semi-axes. We can write Eq. (75) in function of eccentricity of the ellipse with a focus on the origin by replacing a and b terms by r term from Eq. (47). Reducing Eq. (75) by trigonometric identities, the path of the body along of the circular motion, including the rate of apsidal precession traces out an elliptical rosette-like path [Fig. 7(a)], given by

$$\begin{aligned} x' &= \frac{a(1-e^2)}{1-e\cdot\cos(\omega t + d\omega_\varphi t)}\cos(\omega t + \Omega_C t) \\ y' &= \frac{a(1-e^2)}{1-e\cdot\cos(\omega t + d\omega_\varphi t)}\sin(\omega t + \Omega_C t) \end{aligned}, \tag{76}$$

and in polar coordinates, yields

$$r_{Max} = \frac{a(1-e^2)}{1-e\cdot\cos(\omega t + d\omega_\varphi t)}\cos(\omega t + \Omega_C t)\,, \tag{77}$$

where r_{Max} is the maximum distance from the body to the center of rotation (during the aphelion).

REFERENCES

[1] Einstein, A., 1916, Die Grundlage der allgemeinen Relativitätstheorie, Annalen der Physik 49, 770–822.

[2] Schwarzschild, K., 1916, Über das Gravitationsfeld eines Massenpunktes nach der Einsteinschen Theorie. Sitzungsberichte der Königlichen Preußischen Akademie der Wissenschaften zu Berlin 189–196.

[3] Flamm, L., 1916, Beiträge zur Einsteinschen Gravitationstheorie, Physikalische Zeitschrift. 17: 448-454.

[4] Luger, R., Agol, E., Bartolić, F., Foreman-Mackey, D., 2022, Analytic Light Curves in Reflected Light: Phase Curves, Occultations, and Non-Lambertian Scattering for Spherical Planets and Moons, The Astronomical Journal 164, No. 1.

[5] Williams, D.R., 2021, Planetary Fact Sheet – Metric (NASA, Houston, Texas). Retrieved July 16th, 2022.

[6] Einstein, A., 1915, Erklärung der Perihelbewegung des Merkur aus der allgemeinen Relativitätstheorie. Königlich Preußischen Akademie der Wissenschaften (Berlin) 47(2): 831-839.

[7] Cornejo, A. G., 2011, The effect of gravity hypothesis. Lat. Am. J. Phys. Educ. 5(4): 697-701.

[8] Cornejo, A. G., 2014, The Friedmann equations and inflationary cosmology in the effect of gravity hypothesis. Lat. Am. J. Phys. Educ. Vol. 8(4): 4315.1-7.

[9] Riess, A. G., et al., 1998, Observational Evidence from Supernovae for an Accelerating Universe and a Cosmological Constant. The Astron. Jour. 116(3): 1009–1038.

[10] Pain, R., Astier, P., 2012, Observational Evidence of the Accelerated Expansion of the Universe. Comp. Rend. Phys. 13(6): 521–538.

[11] Iorio, L., 2011, General relativistic spin-orbit and spin-spin effects on the motion of rotating particles in an external gravitational field. Gen. Relativ. Gravit. 44:719-736.

[12] Cornejo, A. G., 2014, A Lagrangian solution for the precession of Mercury's perihelion, Int. J. Astron. 3, 31–34.

[13] Cornejo, A. G., 2013, The rotating reference frame and the

precession of the equinoxes, Lat. Am. J. Phys. Educ. 7(4), 591-597.

[14] Cornejo, A. G., 2021, Axial precession in the general theory of relativity solution, Int. J. Astron. 10(1): 1-5.

[15] Cornejo, A. G., 2021, Rotating disk cosmological systems in the Lagrangian and relativistic solutions, Int. J. Astron. 10(2): 50-59.

[16] Lense, J., Thirring, H., 1918, Über die Einfluß der Eigenrotation der Zentralkörper auf die Bewegung der Planeten und Monde nach der Einsteinschen Gravitationstheorie, Zeit. Phys. 19, 156-163.

[17] Williams, D. R., 2018, Sun Fact Sheet, NASA Goddard Space Flight Center. Retrieved July 16th, 2022.

[18] Kerr, R. P., 1963, Gravitational Field of a Spinning Mass as an Example of Algebraically Special Metrics. Physical Review Letters. 11 (5): 237–238.

[19] Lowrie, W., 2007, Fundamentals of Geophysics, 2nd ed. Cambridge University Press.

[20] Cornejo, A. G., 2013, Solution of Einstein's Field Equations for an accelerated magnetic wave. Lat. Am. J. Phys. Educ. 7(2): 217–221.

[21] Mueller, I. I., 1969, Spherical and Practical Astronomy as Applied to Geodesy. Frederick Ungar Publishing, NY, pp. 80.

[22] Malkin, Z., Miller, N., 2009, Chandler wobble: two more large phase jumps revealed. Earth, Planets and Space. 62 (12): 943–947.

[23] Romeo, A. B., Mogotsi, K. M., 2018, Angular momentum and local gravitational instability in galaxy discs: does *Q* correlate with *j* or *M*? Mon. Not. R. Astron. Soc. 000, 1–5.

[24] Konopliv, A. S., Park, R. S., Rivoldini, A., Baland, R. M., Maistre, S. L., Hoolst, T. V., Yseboodt, M., Dehant, V., 2020, Detection of the Chandler Wobble of Mars From Orbiting Spacecraft. Geophysical Research Letters. 47 (21).

[25] Kardar, M., Parisi, G., Zhang, Y., 1986, Dynamic Scaling of Growing Interfaces, Phys. Rev. Lett. 56, 889.

[26] NASA/JPL/Malin Space Science Systems (MSSS), Mars Global Surveyor, May 8, 2003. Retrieved March 18th, 2022.

[27] NASA Science, Share the science, Pictures of Earth from Mars. Mars Global Surveyor, May 8, 2003. Retrieved March 18th, 2022.